

September 28, 2018

Optical Properties of $\text{MFe}_4\text{P}_{12}$ filled skutterudites

S.V. Dordevic⁽¹⁾, N.R. Dilley⁽¹⁾, E.D. Bauer⁽¹⁾, D.N. Basov⁽¹⁾, M.B. Maple⁽¹⁾ and
L. Degiorgi⁽²⁾

⁽¹⁾ *Department of Physics, University of California, San Diego, La Jolla, CA 92093-0319*

⁽²⁾ *Solid State Physics Laboratory HPF-F3/F18, ETH Zürich, CH-8093 Zürich, Switzerland*

Abstract

Infrared reflectance spectroscopy measurements were made on four members of the $\text{MFe}_4\text{P}_{12}$ family of filled skutterudites, with $\text{M}=\text{La}$, Th , Ce and U . In progressing from $\text{M}=\text{La}$ to U the system undergoes a metal-insulator transition. It is shown that, although the filling atom induces such dramatic changes in the transport properties of the system, it has only a small effect on lattice dynamics. We discuss this property of the compounds in the context of their possible thermoelectric applications.

I. INTRODUCTION

Filled skutterudites¹ are a family of compounds with the general structural formula MT_4X_{12} (M =alkaline earth, rare earth, actinide; $\text{T}=\text{Fe}$, Ru , Os ; $\text{X}=\text{P}$, As , Sb). Previous studies have shown that their physical properties are in large part determined by the M atoms. A variety of interesting physical phenomena, including superconductivity, antiferromagnetism, fluctuating valence, and a metal-insulator transition have been observed among the various members of the filled skutterudites²⁻⁷. Recently these compounds attracted renewed attention due to their potential application as thermoelectric materials⁸⁻¹⁰. Mahan

and Sofo¹¹ theorized that optimal thermoelectric properties might be realized for materials which possess a sharp feature in the electronic density of states, which they modeled as a Dirac delta function. Two different approaches have been used in attempts to realize this situation experimentally. One is by reducing the dimensionality of certain materials, as in PbTe/Pb_{1-x}Eu_xTe multiple quantum wells¹². The other approach, which we discuss here, explores electronic f-orbitals of lanthanide atoms, that are almost completely localized in many lanthanide-containing compounds and which give a contribution to the density of states which is a Lorentzian of very narrow width. In searching for materials that satisfy the requirements outlined by Mahan and Sofo, we studied four members of the MFe₄P₁₂ family with M=La, Th, Ce and U as filling atoms.

II. EXPERIMENT

Single crystals of MFe₄P₁₂ compounds were grown in a molten tin flux. High purity (99.9% or better) pieces of the M elements (La, Th, Ce or U), Fe, P and Sn were placed in a quartz tube in the proportions of 1:4:20:50 and sealed under 150 mm of ultra-high purity argon gas. The quartz tube was placed in a furnace and the temperature was elevated to 1050-1150°C. The quartz tube was maintained at this temperature for about a week, and the temperature was then decreased at the rate of 2 °C/h. When the temperature of the furnace reached about 600°C, the quartz tube was dropped into water, and the product of the reaction, consisting of several single crystals embedded in the Sn-P solution, was recovered. These single crystals often grew in the habit of truncated octahedra typical of skutterudite compounds and had dimensions somewhat less than 1x1x1 mm³ (Fig.1, top panel). They could be isolated after etching the Sn-P matrix with a concentrated solution of HCl. The crystal structure of a few of these crystals was verified utilizing Gandolfi or Laue back-reflection x-ray cameras.

Electrical resistivity $\rho_{dc}(T)$ measurements were made using a standard four-probe technique. The shape of the crystals prevented an accurate determination of the sample geometry

and hence of the absolute values of $\rho_{dc}(T)$. Instead the scale of the electrical resistivity data was determined from the room temperature value of the resistivity inferred from the optical measurements. For La and Th-based samples, ρ_{dc} was extracted as the best fit to the Hagen-Rubens formula $R(\omega) = 1 - \sqrt{2\omega\rho_{dc}/\pi}$, whereas for Ce- and U-based samples it was obtained by extrapolating the optical conductivity down to zero frequency.

The electronic structure and charge dynamics in $\text{MFe}_4\text{P}_{12}$ were studied using infrared and optical reflectance spectroscopy. Near normal incidence reflectance $R(\omega)$ of single-crystal samples of $\text{MFe}_4\text{P}_{12}$ was measured at UCSD in the frequency range 50-30,000 cm^{-1} (approximately 5 meV - 3 eV). Single crystal sample of $\text{LaFe}_4\text{P}_{12}$ is shown in the top panel of Fig.1. In our experiments we have collected light reflected by one of the facets of the crystal. To obtain the absolute value of $R(\omega)$ samples were coated in-situ with gold or aluminum in the optical cryostat and the spectrum of a metal-coated sample was used as a reference. This procedure yields reliable absolute values of $R(\omega)$ and does not require ambiguous corrections for diffuse reflectance¹³. Filled skutterudites provide an excellent illustration of the importance of performing optical measurements on natural surfaces. The two La-based samples that were analyzed differed only with respect to the condition of their surface: one of the surfaces was polished, the other was not. A scanning electron microscope (SEM) picture of the sample with natural, unpolished surfaces is shown in Fig.1 (top panel) together with the far infrared (FIR) reflectance of both polished and unpolished samples (bottom panel). Obviously, the polishing procedure significantly damages the surface layer of the sample, as evidenced by the following features in the reflectivity data for the polished sample: (1) a lower overall free-electron reflectance and (2) weaker peaks associated with phonons due to the lack of crystalline long-range order in the surface layer. Fortunately, the procedure for measuring reflectance described above allows us to work with samples of submillimeter size, thus eliminating the need to produce larger surfaces by polishing. The measured frequency interval was extended up to 10eV at ETH on polished specimens of $\text{LaFe}_4\text{P}_{12}$ and $\text{UFe}_4\text{P}_{12}$.

The complex conductivity $\sigma(\omega) = \sigma_1(\omega) + i\sigma_2(\omega)$ and complex dielectric function $\epsilon(\omega) =$

$\epsilon_1(\omega) + i\epsilon_2(\omega)$ were obtained from $R(\omega)$ using a Kramers-Kronig analysis. The uncertainty of the $\sigma(\omega)$ and $\epsilon(\omega)$ spectra due to both low- and high-frequency extrapolations required for the Kramers-Kronig analysis are negligible in the frequency range where the actual data exist.

III. RESULTS

Figure 2 shows the temperature dependence of the electrical resistivity $\rho_{dc}(T)$. The $\text{LaFe}_4\text{P}_{12}$ and $\text{ThFe}_4\text{P}_{12}$ compounds behave like metals, having positive temperature coefficients of resistivity. The residual resistivity ratios $\text{RRR} \equiv \rho(300\text{K})/\rho(4.2\text{K})$ for the two samples are 94 and 1.8, respectively. On the other hand, the resistivities of $\text{CeFe}_4\text{P}_{12}$ and $\text{UFe}_4\text{P}_{12}$ have negative temperature coefficients typical of insulators and semiconductors. The resistivities change by as much as seven orders of magnitude between room temperature and 4.2 K.

Presented in Fig.3 are the raw reflectivity data at room temperature for each of the compounds. As anticipated from transport measurements, $\text{UFe}_4\text{P}_{12}$ shows insulating behavior. The absence of the free electron background allows detailed analysis of the lattice dynamics. Another noticeable feature is relatively high reflectivity ($\sim 40\%$) in the mid-infrared region ($500 - 5,000\text{ cm}^{-1}$). In most insulating compounds $R(\omega)$ does not exceed 10% in this range. We propose that this is a result of the high frequency contribution to the dielectric constant, ϵ_∞ . This behavior seems to be common for all insulating skutterudites, and will be discussed further below.

For $\text{CeFe}_4\text{P}_{12}$, the other known nonmetallic member of the skutterudite family, the reflectances of the two samples analyzed were the same at frequencies $\omega > 300\text{ cm}^{-1}$, but were quite different from each other in the far infrared region. Sample No.1 behaved like a semiconductor (some free electron background is present), whereas sample No.2 was insulating. This sample-to-sample variation was already evident in measurements of both transport and thermodynamic quantities². Since our optical experiments probe the bulk of the crystal¹⁴

and results show significant variations between samples, we conclude that this is a bulk effect. Similar to $\text{UFe}_4\text{P}_{12}$, this material exhibits a high reflectance ($\sim 50\%$) in the mid-infrared part of the spectrum. The increase in reflectivity in the near-infrared and visible is suggestive of interband transitions.

The third member of the family, $\text{ThFe}_4\text{P}_{12}$, displays metallic behavior. The free-electron reflectance is much higher here than in $\text{CeFe}_4\text{P}_{12}$ and $\text{UFe}_4\text{P}_{12}$, but the relatively low plasma edge (around $3,500\text{cm}^{-1}$) is an indication of a low carrier concentration. The increase of the reflectivity in the near-infrared and visible parts of the spectrum is again indicative of interband transitions.

Finally, $\text{LaFe}_4\text{P}_{12}$ is also metallic and exhibits a far-infrared reflectivity that decreases as temperature increases (data not presented in this paper). From transport measurements it is known that this compound is a superconductor with a transition temperature of around 4.2 K ⁵. The general shape of the reflectivity is the same as in $\text{ThFe}_4\text{P}_{12}$. The only difference between the two is in the position of the "plasma minimum" in $R(\omega)$, which is shifted to about $4,000\text{ cm}^{-1}$ in $\text{LaFe}_4\text{P}_{12}$ (see Fig.3).

The next step in the analysis is to perform a Kramers-Kronig transformation on the raw reflectivity data. To do that one needs to extrapolate the reflectivity to the regions where the actual data are not available. For electrically conducting samples ($\text{LaFe}_4\text{P}_{12}$ and $\text{ThFe}_4\text{P}_{12}$), high FIR reflectance suggests using a Hagen-Rubens (HR) extrapolation (commonly used for metals): $R(\omega) = 1 - \sqrt{2\omega\rho_{dc}/\pi}$, where ρ_{dc} is the only parameter of the model. The natural way to proceed is to use ρ_{dc} from transport measurements and calculate $R(\omega)$. But since ρ_{dc} was not available, we inverted the procedure: we found the best fit to the reflectance data and used it to calculate the absolute values of our transport measurements (Fig.2). The best fits for $\text{LaFe}_4\text{P}_{12}$ and $\text{ThFe}_4\text{P}_{12}$ were 85 and $200\ \mu\Omega\text{cm}$, respectively. A power law extrapolation $R(\omega) \sim 1/\omega^4$ was used for high frequencies. For the $\text{CeFe}_4\text{P}_{12}$ and $\text{UFe}_4\text{P}_{12}$ samples, we extrapolated the low frequency part with a straight line: for the semiconducting $\text{CeFe}_4\text{P}_{12}$ sample perfect reflectance at zero frequency was assumed (suggested by the tendency of the data), whereas for the insulating $\text{CeFe}_4\text{P}_{12}$ and $\text{UFe}_4\text{P}_{12}$ compounds we assumed a constant

reflectance (horizontal straight line). For the high frequency part the same power law as before was used.

Using these extrapolations, the Kramers-Kronig transformation was performed and the frequency dependence for the complex conductivity $\sigma(\omega)$ and complex dielectric function $\epsilon(\omega)$ were obtained. Figure 4 shows results for the real part of the conductivity $\sigma_1(\omega)$. Characteristics anticipated from reflectance data are now obvious: $\text{LaFe}_4\text{P}_{12}$ and $\text{ThFe}_4\text{P}_{12}$ are metallic, one of the $\text{CeFe}_4\text{P}_{12}$ samples is semiconducting while the other is insulating¹⁵, and, finally, $\text{UFe}_4\text{P}_{12}$ is insulating.

Conductivity spectra for $\text{LaFe}_4\text{P}_{12}$ and $\text{ThFe}_4\text{P}_{12}$ are clearly Drude-like, but we failed to obtain good fits to the formula $\sigma_1(\omega) = \sigma_0/(1 + \omega^2\tau^2)$. Instead, spectra were analyzed within the “extended” Drude model. Here one allows for the frequency dependence of the scattering rate $1/\tau$. It can be shown¹⁶ that causality requires the effective mass to be frequency dependent as well. The spectra of the quasiparticle effective mass $m^*(\omega)/m_e$ (m_e - electron band mass) and scattering rate $1/\tau(\omega)$ can be obtained from the optical conductivity:

$$\frac{m^*(\omega)}{m_e} = \frac{\omega_p^2}{4\pi} \frac{\sigma_2(\omega)}{\sigma_1^2(\omega) + \sigma_2^2(\omega)} \frac{1}{\omega} \quad (1)$$

$$\frac{1}{\tau(\omega)} = \frac{\omega_p^2}{4\pi} \frac{\sigma_1(\omega)}{\sigma_1^2(\omega) + \sigma_2^2(\omega)} \quad (2)$$

where the plasma frequency $\omega_p^2 = 4\pi ne^2/m_e$ is estimated from the integration of $\sigma_1(\omega)$ up to the frequency corresponding to the onset of the interband absorption. When these equations are used to describe the response of a conventional metal one finds that both the scattering rate and effective mass are independent of frequency. The results of the analysis for $\text{LaFe}_4\text{P}_{12}$ and $\text{ThFe}_4\text{P}_{12}$ are presented in Fig.5 (top and bottom panel, respectively). For both compounds the effective mass (right panels) is only slightly enhanced ($m^*/m_e < 5$) and almost temperature independent. The scattering rate (left panels) is linear in frequency (up to 3000 cm^{-1} for $\text{LaFe}_4\text{P}_{12}$ and 2000 cm^{-1} for $\text{ThFe}_4\text{P}_{12}$) and is temperature dependent. The values obtained by extrapolating the curves down to zero frequency (*dc* limit) are plotted in

Fig.2 as full squares (for $\text{LaFe}_4\text{P}_{12}$) and full circles (for $\text{ThFe}_4\text{P}_{12}$). Such a good scaling is not surprising if one considers the relation $\rho_{dc} = m^*/ne^2\tau$ and the fact that effective mass m^* and carrier concentration n are temperature independent. A huge factor of 50 difference in the residual resistivity ratio RRR between La and Th-based samples is consistent with the temperature dependence of the scattering rate. At low temperature the phonon contribution is strongly suppressed and the large residual scattering in this region for $\text{ThFe}_4\text{P}_{12}$ indicates that the La-based sample was much “cleaner”.

Figure 6 displays the real part of the complex dielectric function $\epsilon_1(\omega)$ up to $3,000\text{ cm}^{-1}$ (0.3eV) for all the samples, where contributions from the interband transitions at higher frequencies are not shown. Also shown are the resonance plasma frequencies ω_p^* (determined as zero crossings of $\epsilon_1(\omega)$) for the $\text{LaFe}_4\text{P}_{12}$, $\text{ThFe}_4\text{P}_{12}$ and semiconducting $\text{CeFe}_4\text{P}_{12}$, and high-frequency contributions ϵ_∞ for the insulating $\text{CeFe}_4\text{P}_{12}$ and $\text{UFe}_4\text{P}_{12}$.

IV. DISCUSSION

A. Electronic Properties

Electronic properties of both filled and unfilled skutterudites have been discussed in a number of publications^{1,17–19}. The filling atom is always assumed to be positively charged and only weakly bound to the transition-metal pnictogen polyanion. The bonds within the polyanion are considered to be covalent. A simple charge counting method is sometimes used to predict the properties of the compounds. According to this method, the polyanion $[\text{Fe}_4\text{P}_{12}]^{4-}$ should be isoelectronic with CoP_3 (Co_4P_{12}) which is semiconducting. The electronic properties of $\text{MFe}_4\text{P}_{12}$ will therefore depend on the valence state of the filling atom M. Metallic behavior is indeed observed in $\text{MFe}_4\text{P}_{12}$ where $\text{M} = \text{La}, \text{Pr}, \text{Nd}, \text{Sm}, \text{or Eu}$ is trivalent, and semiconducting behavior in $\text{CeFe}_4\text{P}_{12}$ and $\text{UFe}_4\text{P}_{12}$, where U and Ce may be tetravalent. However, there is growing consensus that f-electron hybridization effects better explain the semiconducting behavior in latter materials^{20–22}, as we discuss later in

this paper. Furthermore, the charge counting arguments fail to predict the correct behavior for $\text{ThFe}_4\text{P}_{12}$, in which Th is believed to be tetravalent¹⁸ and is therefore expected to make the compound semiconducting (electronically saturated). Both the frequency (Fig.4) and temperature (Fig.2) dependence of the conductivity clearly demonstrate metallic behavior. This simple charge counting method thus seems insufficient to explain all the experimental results, and more detailed band structure calculations are necessary.

The absolute values of the resistivity data for the metallic samples (Fig.2, top panel) are approximately two orders of magnitude higher than in typical metals. Apparently the curve for the Th-based sample exceeds the value of $150 \mu\Omega\text{cm}$, which is the so-called Ioffe-Regel limit. In conventional metals it corresponds to the regime when the carrier mean free path is approaching the lattice constant. The value of $150 \mu\Omega\text{cm}$ is calculated for conventional metals, where $n \sim 10^{22}\text{cm}^{-3}$, $\tau \sim 10^{-14}\text{s}$ and $m^*/m_e = 1$. From the plasma frequency ω_p we estimated the carrier concentration in the Th-based sample to be approximately two orders of magnitude lower ($n \sim 10^{20}\text{cm}^{-3}$) which places the Ioffe-Regel limit for this compound much higher. The spectra of the dielectric constant (Fig.6) of $\text{LaFe}_4\text{P}_{12}$ and $\text{ThFe}_4\text{P}_{12}$ also exhibit the characteristics of “poor” metals. The zero crossing of the dielectric constant, which determines the plasma resonance frequency:

$$\omega_p^* = \frac{\omega_p}{\sqrt{\epsilon_\infty}} = \sqrt{\frac{4\pi n e^2}{m_e \epsilon_\infty}} \quad (3)$$

is in the range 0.1-0.3eV, confirming a low carrier concentration for both compounds.

Besides having low carrier concentration, these compounds also seem to have an unusual frequency dependence of the carrier scattering rate: $1/\tau \sim \omega$ (Fig.5, left panels). We believe that this is caused by the interband transitions that are at relatively low frequencies (around $10,000\text{cm}^{-1}$, Fig.4) and contribute considerably even below 1000cm^{-1} . The interband transitions also affect the effective mass: they drive it below the free electron mass, and even to negative values (Fig.5, right panels).

On the other hand, $\text{UFe}_4\text{P}_{12}$ and $\text{CeFe}_4\text{P}_{12}$ display all the characteristics of insulators or semiconductors. High values of ϵ_∞ (17 for $\text{UFe}_4\text{P}_{12}$, 31 for $\text{CeFe}_4\text{P}_{12}$ No.1 and 32 for

CeFe₄P₁₂ No.2, see Fig.6) are typical for hybridization gap semiconductors^{23,24}, as explained later in the text. This results in the anomalously large mid-infrared reflectance that was mentioned above. Model calculations of reflectivity for several different values of ϵ_∞ are presented in Fig.7. The other parameters of the model, obtained as the best fit to the reflectance spectrum of the U-based sample, were kept constant. It is apparent that the increase of ϵ_∞ leads to the enhancement of the absolute value of $R(\omega)$ in the mid-infrared.

All conductivity spectra show a broad maximum centered around 1.5eV (Fig.4), a signature of an interband transition. At this moment, band structure calculations are available for Ce and La-based compounds only^{20–22}, and they do not show any characteristic feature at this energy range. For CeFe₄P₁₂ a gap at the Fermi level of about 0.34eV is predicted²², but our spectrum indicates a somewhat smaller value of about 0.15eV. This value is also consistent with the activation energy obtained from fitting resistivity measurements to an activation conduction form, $\rho = \rho_0 \exp(\Delta E / k_B T)$, in the temperature range $80\text{K} < T < 150\text{K}$ which yields an activation energy ΔE of around 0.13eV². One possible origin of the insulating behavior which has been previously put forward² is hybridization between the f electron orbitals present in UFe₄P₁₂ and CeFe₄P₁₂ with the conduction electrons which opens a gap in the electronic density of states at the Fermi energy. This would be analogous to the hybridization gap seen in the intermediate valent systems SmB₆ and SmS²⁵, except that the latter materials have considerably smaller activation energies than CeFe₄P₁₂. Band structure calculations²² also suggest that Ce 4*f* states hybridize strongly with Fe 3*d* and phosphorus *p* states in the vicinity of the Fermi level. The notion of hybridization is also supported by the experimental findings presented in this paper. Namely, hybridization gap semiconductors are predicted²³ to have: (1) high values of ϵ_∞ and (2) anomalously large values of Born effective charges (explained below). We indeed find experimental evidence for both of these effects. As La and Th do not have any f electrons, no hybridization takes place, and thus LaFe₄P₁₂ and ThFe₄P₁₂ display metallic behavior. Clearly, additional theoretical and computational work is required to explain these experimental findings in metallic skutterudites.

B. Phonon Spectra

Filled skutterudites crystallize in the cubic structure (space group $Im\bar{3} - T_h^{26}$). Applying the correlation method²⁷, the following decomposition into the irreducible representations is obtained: $\Gamma = 2A_g + 2E_g + 4F_g + 2A_u + 2E_u + 8F_u$. Eight of these modes are infrared active (F_u species), eight are Raman active (A_g , E_g and F_g species) and the other are neither infrared nor Raman active. All infrared active modes are triply degenerate.

Frequencies and oscillator strengths of all phonon modes identified in the conductivity spectra are given in Table 1. The numerical values are obtained as the best fits in the classical oscillator model²⁸:

$$\sigma_{ph}(\omega) = \frac{1}{4\pi} \sum_j \frac{S_j \gamma_j \omega^2}{(\omega_j^2 - \omega^2)^2 + \gamma_j^2 \omega^2} \quad (4)$$

Although the group theory analysis predicts eight infrared active modes, we were able to identify only six from the spectra of the insulating samples. The oscillator strength of the other two was probably below our detection limits. Due to a high free-electron contribution to the conductivity, only four phonons are identified in the Th-based sample and three in the La-based sample. Interestingly, except for the lowest lying mode, all peaks are at nearly the same frequency in all compounds. We propose below that they are due to the Fe_4P_{12} sublattice. The filling ion M is believed not to be very strongly bound to this sublattice and is free to rattle within the "cage". Weak binding could be the reason for the high oscillator strength of this mode (Table.1) The most interesting feature of the phonons is that even though the conductivity (carrier concentration) changes by almost three orders of magnitude going from the U to La samples, the oscillator strength of the phonon modes is only weakly affected (Table 1). Despite the fact that the conductivity of "metallic" samples is enhanced, the carrier density is still below 0.2 electrons/unit cell which is much lower than the effective oscillating charge.

C. Effective Charges

The discussion in Section IV.A suggests that the metal-insulator transition in the $\text{MFe}_4\text{P}_{12}$ series is in accord with the opening of a hybridization gap in the electronic density of states. Another predicted feature of the hybridization gap semiconductors are anomalously high values of the effective dynamic charges²³. Our calculations of the Born dynamical charges $e_B^*(M)$ for U and Ce-based samples are indeed in agreement with this prediction. The Born effective charge can be determined from the formula:

$$\sum_j \left(\omega_{LO,j}^2 - \omega_{TO,j}^2 \right) = \frac{Z e_B^{*2}(m)}{V_B c^2 \pi \epsilon_\infty m} \quad (5)$$

where $\omega_{LO,j}$ and $\omega_{TO,j}$ are frequencies of the longitudinal and transverse optical phonons, respectively, V_B is the volume of the primitive cell, Z is the number of formula units in the primitive cell ($Z=2$) and m is the reduced mass of the primitive cell.

In accord with our assignment of phonons in the previous section, we calculate e_B^* for the filling ion and Fe_4P_{12} sublattice separately. For the former, the sum on the left-hand side of Eq.5 has only one term (the lowest lying phonon), whereas for the latter it runs over all the remaining peaks. This procedure gives the following results for the Fe_4P_{12} sublattice: $e_B^*=8.9$ in $\text{UFe}_4\text{P}_{12}$ and 11 in $\text{CeFe}_4\text{P}_{12}$. Such high values for a predominantly covalent lattice (covalent bonding is expected within the Fe_4P_{12} polyanion) indicate that hybridization plays an important role. The dynamical charge associated with the filling ion is also anomalously high. For U and Ce-based samples we find e_B^* of 8.9 and 8.7, respectively. Obviously, such high values of the transverse dynamical charge (i.e., the one that couples to the external radiation and that is measured in optical experiments) cannot be due to the valence state of the ionically bonded filling atoms.

D. Thermoelectric Applications

There has been an enormous amount of research in the field of thermoelectric materials in the recent years, with emphasis on novel materials concepts. The figure of merit of a

material for thermoelectric applications is measured by the dimensionless quantity:

$$ZT = \frac{\sigma S^2}{\kappa_e + \kappa_l} T \quad (6)$$

where T is temperature, σ is the electrical conductivity, S is the Seebeck coefficient and κ_e and κ_l are electronic and lattice contributions to the thermal conductivity. For the novel TE materials to be competitive with conventional cooling systems, $ZT \approx 3$ is required⁸. The filled skutterudites (e.g., $\text{LaFe}_3\text{CoSb}_{12}$ and $\text{CeFe}_3\text{CoSb}_{12}$) attracted attention as potential thermoelectric materials because it was shown that they exhibit large Seebeck coefficients typical of semiconductors yet have moderately high electrical conductivity and also very low lattice thermal conductivity κ_l ^{8,10,29}. The latter property has been attributed to the localized, incoherent vibrations (rattling) of the filling ions within the atomic "cages" formed by the other atoms. The hypothesis was based on ultrasound, neutron diffraction, and specific heat measurements, and on the fact that κ_l for the unfilled skutterudite CoSb_3 was several times larger at all temperatures³⁰.

We believe that the lowest lying phonon (which varies in frequency from compound to compound) is this rattling mode. All other phonons can be attributed to the dynamics of the Fe_4P_{12} sublattice, which explains their similarity in all four compounds (both in frequency and in strength). It has been recently suggested^{30,31} that the rattling of the filling ion can be treated as a localized vibrational mode. We note that in $\text{UFe}_4\text{P}_{12}$ and $\text{CeFe}_4\text{P}_{12}$ the frequencies of the lowest lying mode scale as $\sqrt{k/M}$, where M is the mass of the filling ion and k is the force constant, found to be the same in Ce and U-based crystals. This scaling suggest that the filling ion is weakly bound to the lattice. If the filling ion were strongly bound to the lattice, one would expect the force constant to be quite different for different ions. Based on the calculated value of the force constant we estimate the phonon frequencies for the same mode in $\text{ThFe}_4\text{P}_{12}$ and $\text{LaFe}_4\text{P}_{12}$. They are expected to be around 82 and 141 cm^{-1} , respectively (indicated by arrows in Fig.3). The free electron background in raw reflectance data in this frequency range for these two compounds is too high to allow detection of any phonons.

In order to produce viable thermoelectric materials, careful tuning of the compound's carrier concentration is required. Several alloying schemes are possible within the filled skutterudites. Compounds of the form $M(T_xT'_{4-x})X_{12}$, $MT_4(X_yX'_{12-y})$ or even $M(T_xT'_{4-x})(X_yX'_{12-y})$ have been successfully synthesized^{8,10,29}. Recently compounds of the form $La_{1-x}Ce_xRu_4P_{12}$ ($0 \leq x \leq 1$) were produced at high pressures³², demonstrating the ability to vary x continuously over the entire alloying range. We believe that this may allow us to design a material whose electrical and thermal conductivities are optimal for thermoelectric applications.

Finally, we want to discuss our experimental results from the point of view of Mahan and Sofo's theory¹¹. They point out that all transport coefficients relevant for thermoelectric materials (σ , S and κ_e) are functions of the electronic density of states $N_{el}(E)$. They find, in the case of a material with the minimum lattice thermal conductivity $\kappa_l \approx 2mW/(cmK)$, that a sharp feature (theoretically a Dirac delta function) in the electronic density of states located $2.4k_B T$ away from the Fermi level is needed to maximize ZT . This is equivalent to having a resonance approximately 60meV (at room temperature) above or below the Fermi level. None of the materials we have analyzed in this paper shows any characteristic feature on this energy scale (Fig.4). We are currently studying another member of the skutterudites family, $YbFe_4Sb_{12}$ ⁷, and find interesting charge dynamics in the anticipated energy range³³.

V. CONCLUSIONS

We have presented evidence in this paper that transport and optical properties of the filled skutterudites are primarily determined by the filling ion. The experimental results support the idea that hybridization plays an essential role in determining the properties of the MFe_4P_{12} compounds. From the optical spectrum of samples with $M = Ce$ and U , we inferred the following properties: (1) a gap in the electronic density of states, (2) a large value of the dynamical effective charges, and (3) an enhanced dielectric constant at high frequencies ϵ_∞ . Localized, incoherent vibrations ("rattling") of the filling ions were

successfully modeled as Einstein oscillators, in agreement with recent reports^{30,31,34}. Atomic substitutions at this site will not only tailor the electrical conductivity of the material but may also increase the phonon scattering due to the rattling of the various filling ions. We believe that this method (atomic substitution at the filling atom site), combined with alloying at the Fe and P sites, opens possibilities for significant improvements of the thermoelectric coefficient. Further research, especially measurements of thermal conductivity, is needed to verify these ideas.

VI. ACKNOWLEDGEMENTS

Research at UCSD was supported by the U.S. Department of Energy under Grant No. DE-FG03-86ER-45230, the U.S. National Science Foundation under Grants No. DMR-97-05454 and DMR-98-75-980, the Campus Laboratory Collaboration of the University of California and Sloan Foundation. D.N.B is a Cottrell Fellow of the Research Corporation.

REFERENCES

- ¹ W. Jeitschko and D. Braun, Acta Crystallographica, Section B (Structural Crystallography and Crystal Chemistry) **B33** pt.11, 3401-6 (1977)
- ² G.P. Meisner, M.S. Torikachvili, K.N. Yang, M.B. Maple and R.P. Guertin, J.Appl.Phys. **57**, (1) 3073, (1985)
- ³ M.S. Torikachvili, J.W. Chen, Y. Dalichaouch, P.P. Guertin, M.W. McElfresh, C. Rossel, M.B. Maple and G.P. Meisner, Phys.Rev B, **36**, 8860-4, (1987)
- ⁴ L.E. DeLong and G.P. Meisner, Solid State Communications, Vol.**53**, No.2, pp. 119-123, (1985)
- ⁵ G.P. Meisner, Physica **108B**, 763-4, (1981)
- ⁶ I. Shirotni, T. Uchiumi, K. Ohno, C. Sekine, Y. Nakazawa, K. Kanada, S. Todo and T. Yagi, Phys.Rev.B **56**, No.13, 7866-9, (1997)
- ⁷ N.R. Dilley, E.J.Feeman, E.D.Bauer and M.B.Maple, Phys.Rev.B **58**, No.10, 6287-90, (1998)
- ⁸ G. Mahan, B. Sales and J. Sharp, Physics Today, 42-7, March 1997
- ⁹ G.A. Slack and V.G. Tsoukala, J.Appl.Phys., **76** (3) 1665-71, (1994)
- ¹⁰ G.S. Nolas, G.A. Slack, D.T. Morelli, T.M. Tritt and A.C. Ehrlich, J.Appl.Phys. **79** (8) 4002-8, (1996)
- ¹¹ G.D. Mahan and J.O. Sofo, Proc.Nat.Acad.Sci.USA, Vol.**93**, 7436-9, (1996)
- ¹² T.Koga, S.B.Cronin, T.C.Harman, X.Sun and M.S.Dresselhaus, Mater.Res.Soc.Symp. Proc., Vol.**490**, 263-8, (1998)
- ¹³ C. Homes, M.A. Reedyk, D.A. Crandels and T. Timusk, Applied Optics **32**, 2976 (1993)
- ¹⁴ Our estimates based on σ_{dc} suggest that IR radiation probes the crystal to a depth of at

least 5-10 μm .

- ¹⁵ Due to the unusual phonon structure in the spectrum, we have not been able to complete Kramers-Kronig analysis for $\text{CeFe}_4\text{P}_{12}$ samples (we obtained physically unrealistic negative values for conductivity). Instead, we fitted the reflectance spectra and, using the same parameters, generated the conductivity and dielectric constant spectra which are shown as thin lines in Fig.4 and 6. The free-electron part was fitted with the Drude formula and the phonons were modeled as Lorentzian oscillators.
- ¹⁶ D.B.Tanner and T.Timusk in *Physical Properties of High Temperature Superconductors III*, edited by D.M.Ginsberg (World Scientific, 1993)
- ¹⁷ F.Grandjean, A.Gerard, D.J.Braun and W.Jeitschko, J.Phys.Chem.Solids Vol. **45**, No.8/9, 877-86, (1984)
- ¹⁸ M.E.Danebrock, C.B.H.Evers and W.Jeitschko, J.Phys.Chem.Solids, Vol.**57**, No.4, 381-7, (1996)
- ¹⁹ C.B.H. Evers, W. Jeitschko, L. Boonk, D.J. Braun, T. Ebel and U.D. Scholz, Journal of Alloys and Compounds, **224**, 184-9, (1995)
- ²⁰ D.J. Singh, L. Nordstrom, W.E. Pickett and J.L. Feldman, 15th International Conference on Thermoelctetics (1996)
- ²¹ D.J. Singh and I.I. Mazin, Phys.Rev.B, **56**, R1650-3, (1997)
- ²² L. Nordström and D.J. Singh, Phys.Rev.B **53** 1103-8 (1996)
- ²³ S. Ögüt and K.M. Rabe, Phys.Rev.B **54**, No.12, R8297-300, (1996)
- ²⁴ A. Damascelli, K. Schulte, D. van der Marel and A.A. Menovsky, Phys.Rev.B, Vol.**55**, No.8, R4863-6, (1997)
- ²⁵ *Valence Fluctuations in Solids*, edited by L.M.Falicov, W.Hanke and M.B.Maple (North-Holland, Amsterdam, 1981)

- ²⁶ H.D. Lutz and G. Kliche, Phys.Stat.Sol (b), **112**, 549 (1982)
- ²⁷ W.G. Fateley, F.R. Dollish, N.T. McDevitt and F.F. Bentley *Infrared and Raman Selection Rules for Molecular and Lattice Vibrations: The Correlation Method* (Wiley-Interscience, New York, 1972)
- ²⁸ P.Brüesch, *Phonons: Theory and Experiment* (Springer, New York, 1982), Vols.1 and 2.
- ²⁹ B. Chen, J. Xu, C. Uher, D.T. Morelli, G.P. Meisner, J. Fleurial, T. Caillat and A. Borchevski, Phys.Rev. **55**, No.3., 1476-80, (1997)
- ³⁰ V. Keppens, D. Mandrus, B.C. Sales, B.C. Chakoumakos, P. Dai, R. Coldea, M.B. Maple, D.A. Gajewski, E.J. Freeman and S. Bennington, Nature, vol.**395**, 876-8, (1998)
- ³¹ D. Mandrus, B.C. Sales, V. Keppens, B.C. Chakoumakos, P. Dai, L.A. Boatner, R.K. Williams, J.R. Thompson, T.W. Darling, A. Migliori, M.B. Maple, D.A. Gajewski and E.J.Freeman, Mat.Res.Soc.Symp.Proc., Vol.**478**, 199-209, (1997)
- ³² I. Shiotani, T. Uchiumi, C. Sekine, M. Hori and S. Kimura, Journal of Solid State Chemistry, **142**, 146-51, (1999)
- ³³ S. Dordevic, N.R. Dilley, D.N. Basov, E.D. Bauer and M.B. Maple, to be published, (1999)
- ³⁴ J.L. Feldman, D.J. Singh and I.I. Mazin, to be published, (1999)

FIGURES

FIG. 1. An SEM picture of as-grown $\text{LaFe}_4\text{P}_{12}$ single crystal (top panel). Reflectance spectra (bottom panel) show the importance of natural surfaces; polishing damages the surface layer of the sample, creating defects that increase resistivity (lower the reflectance). The phonons are also much weaker due to the lack of long range order.

FIG. 2. Temperature dependence of the dc resistivities of $\text{MFe}_4\text{P}_{12}$. The absolute values are obtained by extrapolating the optical conductivity down to zero frequency (for U- and Ce-based samples) and from the Hagen-Rubens fits to the reflectance (for Th- and La-based samples). Also shown is the Ioffe-Regel limit calculated for $n \sim 10^{22} \text{ cm}^{-3}$ (typical for conventional metals). In $\text{ThFe}_4\text{P}_{12}$ the carrier concentration is two orders of magnitude lower, placing the Ioffe-Regel limit much higher. The carrier scattering rate (right-hand axis in the top panel), is shown as full circles for $\text{LaFe}_4\text{P}_{12}$ and full squares for $\text{ThFe}_4\text{P}_{12}$. These values are obtained by extrapolating the scattering rate to zero frequency (see Fig.5).

FIG. 3. Reflectance spectra of four members of the skutterudite family. The arrows on the graphs for La and Th samples indicate the positions of the "rattling" mode, calculated from the simple harmonic model (see text for details).

FIG. 4. Real part of the optical conductivity as obtained from a Kramers-Kronig analysis. All spectra show a broad maximum around 1.5eV, which we attribute to an interband transition. The low frequency part of the $\text{CeFe}_4\text{P}_{12}$ spectra (thin lines) is obtained by fitting the reflectance data.

FIG. 5. Frequency dependent effective mass (right panels) and scattering rate (left panels) obtained within the "extended" Drude formalism of Eq.1 and Eq.2 (see text), applied to $\text{LaFe}_4\text{P}_{12}$ (top panels) and $\text{ThFe}_4\text{P}_{12}$ (bottom panels). Note a slight mass enhancement and linear frequency dependence of the scattering rate.

FIG. 6. Real part of the dielectric function, shown over a narrower frequency range (up to about 0.3eV). Again, thin lines are used for the simulated region (for $\text{CeFe}_4\text{P}_{12}$). The low values of the plasma resonance frequency ω_p^* are an indication of low carrier concentrations. The high frequency contributions to the dielectric function (ϵ_∞) for insulating Ce and U-based samples are also shown. High values are typical of hybridization gap semiconductors.

FIG. 7. Model calculations of the reflectance for $\text{UFe}_4\text{P}_{12}$, shown for several values of the free parameter ϵ_∞ . The phonon parameters ν_j and ρ_j for these curves are given in Table 1. Apparently, an increase in ϵ_∞ leads to an increase in the mid-infrared reflectance.

TABLES

TABLE I. Frequency ω_j in cm^{-1} and reduced oscillator strength $\rho_j = S_j/4\pi\omega_j$ (in parentheses) of infrared active phonon modes at $\mathbf{q}\approx\mathbf{0}$ obtained by a fit to the classical oscillator model.

	ν_1	ν_2	ν_3	ν_4	ν_5	ν_6
LaFe ₄ P ₁₂			294 (0.08)	325 (0.08)	376 (0.22)	
ThFe ₄ P ₁₂		257 (0.14)	304 (0.20)	337 (0.11)	393 (0.73)	
CeFe ₄ P ₁₂	104 (1.17)	255 (0.07)	305 (0.14)	338 (0.13)	396 (0.51)	414 (0.01)
UFe ₄ P ₁₂	80 (1.27)	256 (0.13)	308 (0.12)	339 (0.10)	397 (0.22)	411 (0.03)

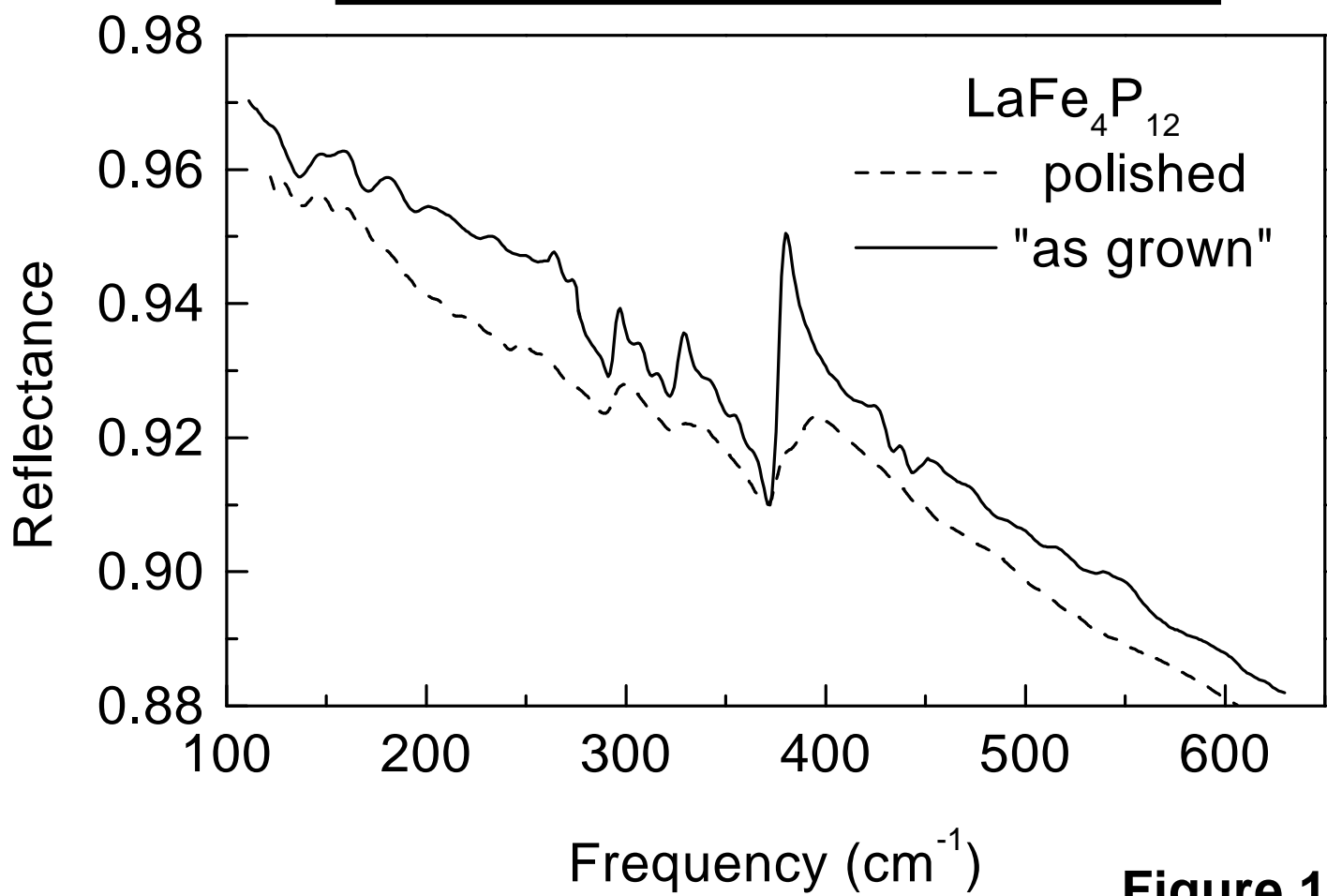
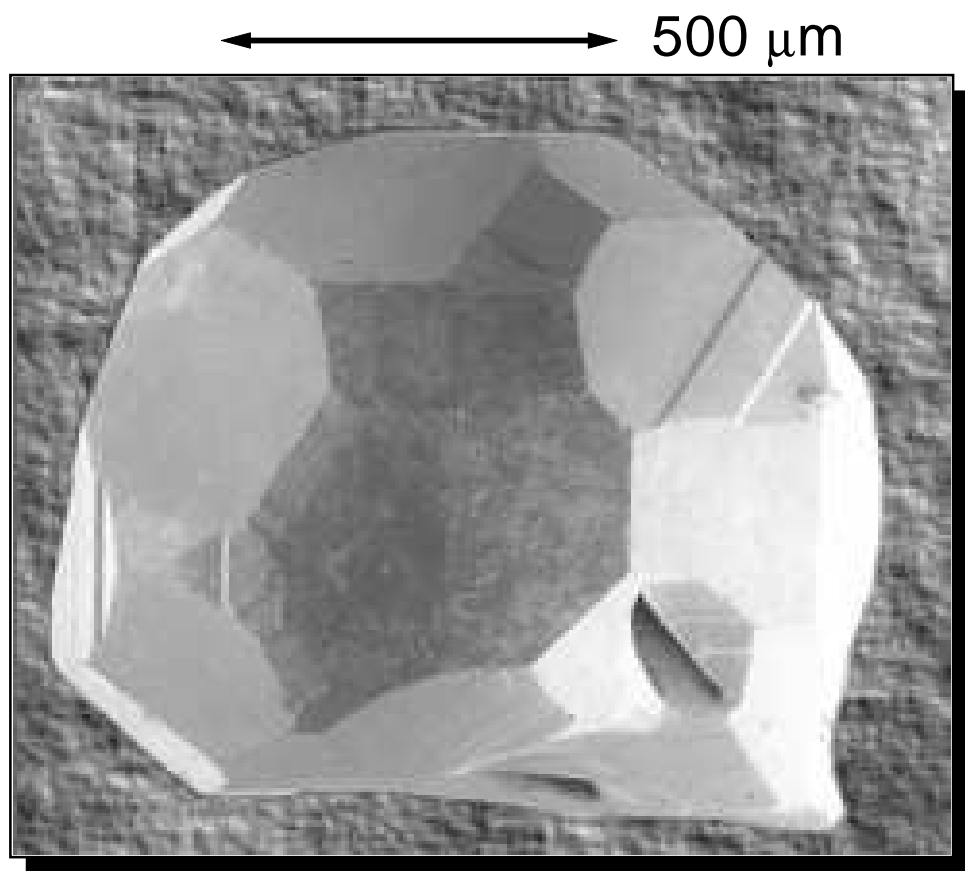


Figure 1

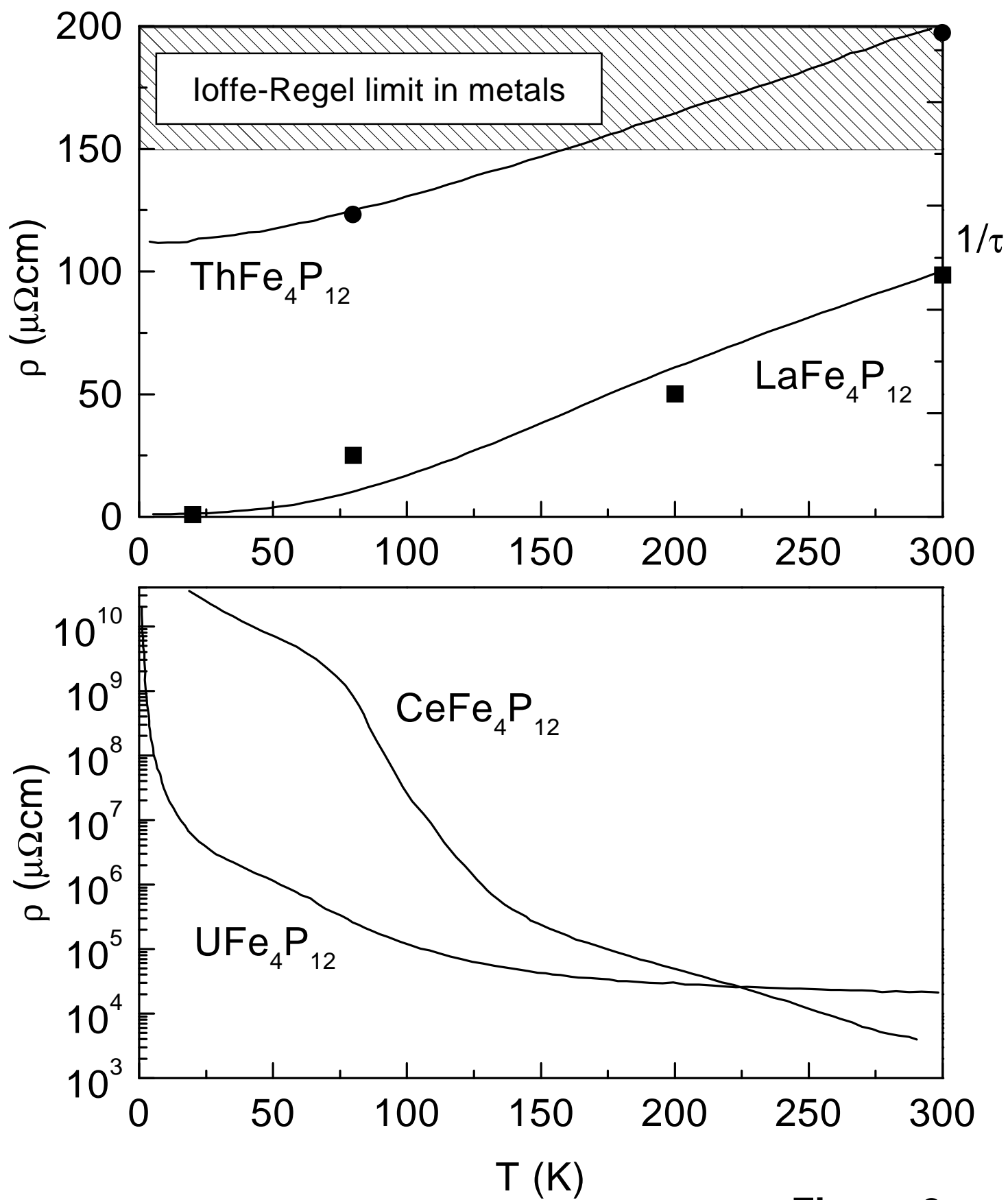


Figure 2

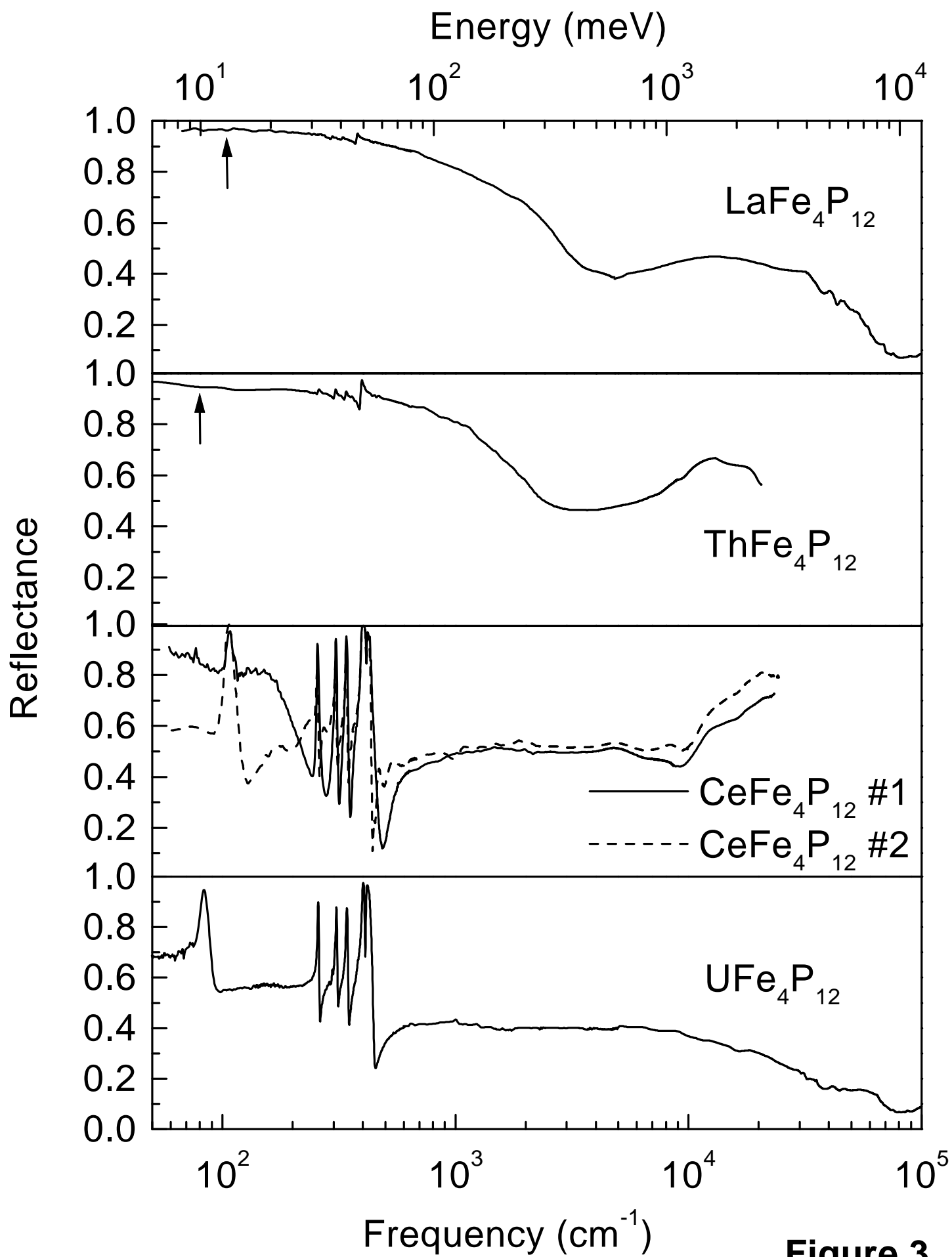


Figure 3

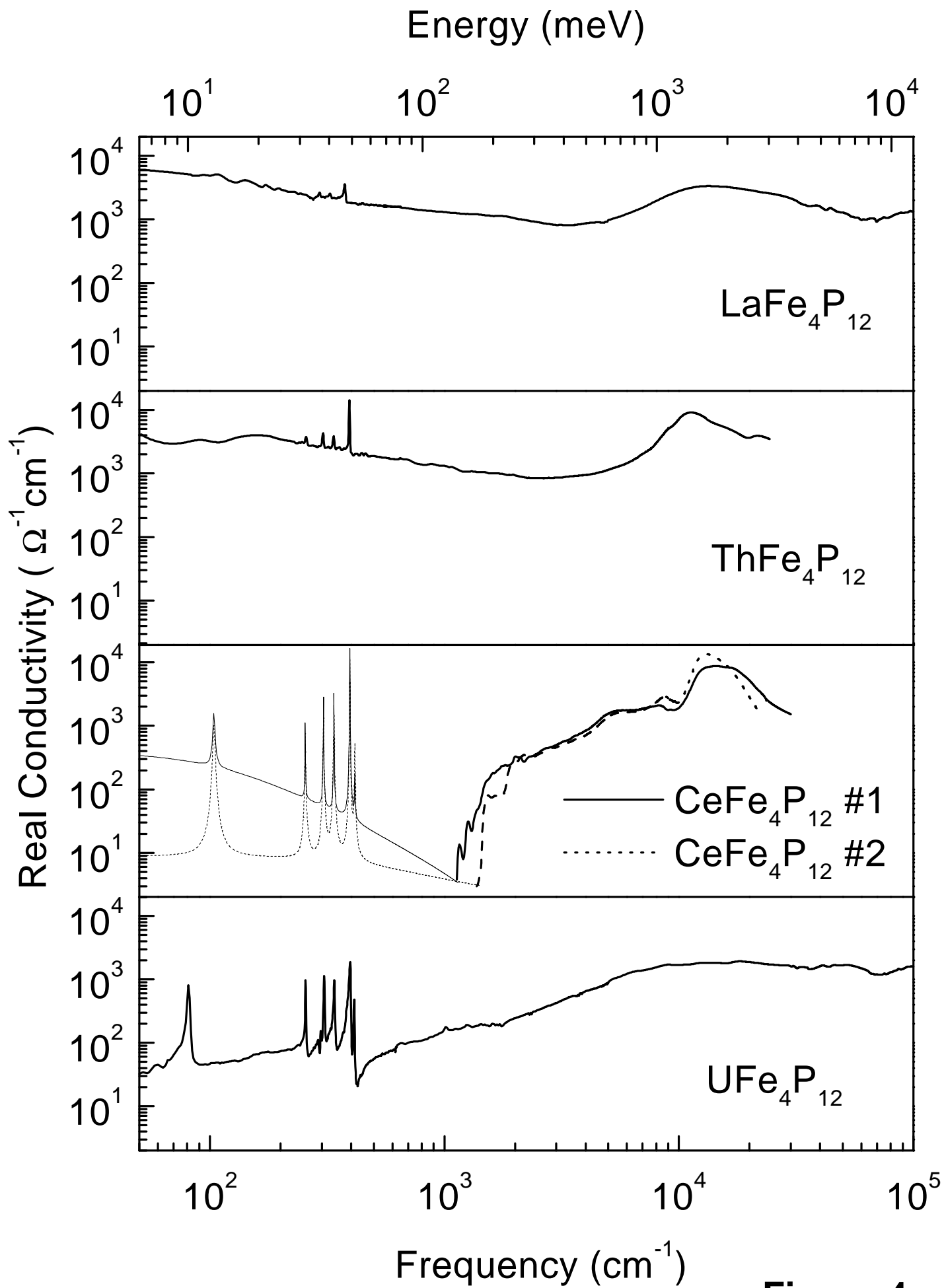


Figure 4

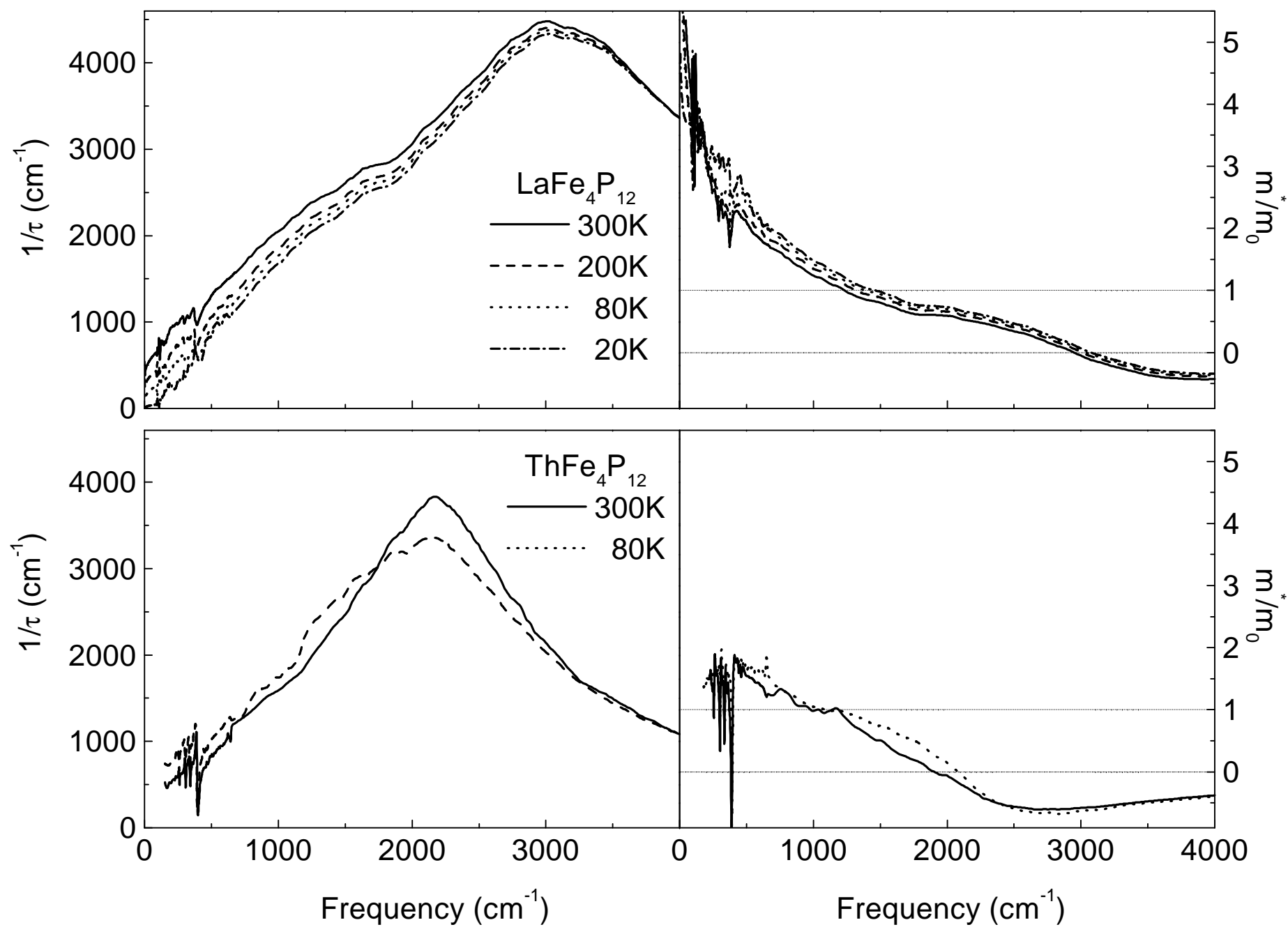


Figure 5

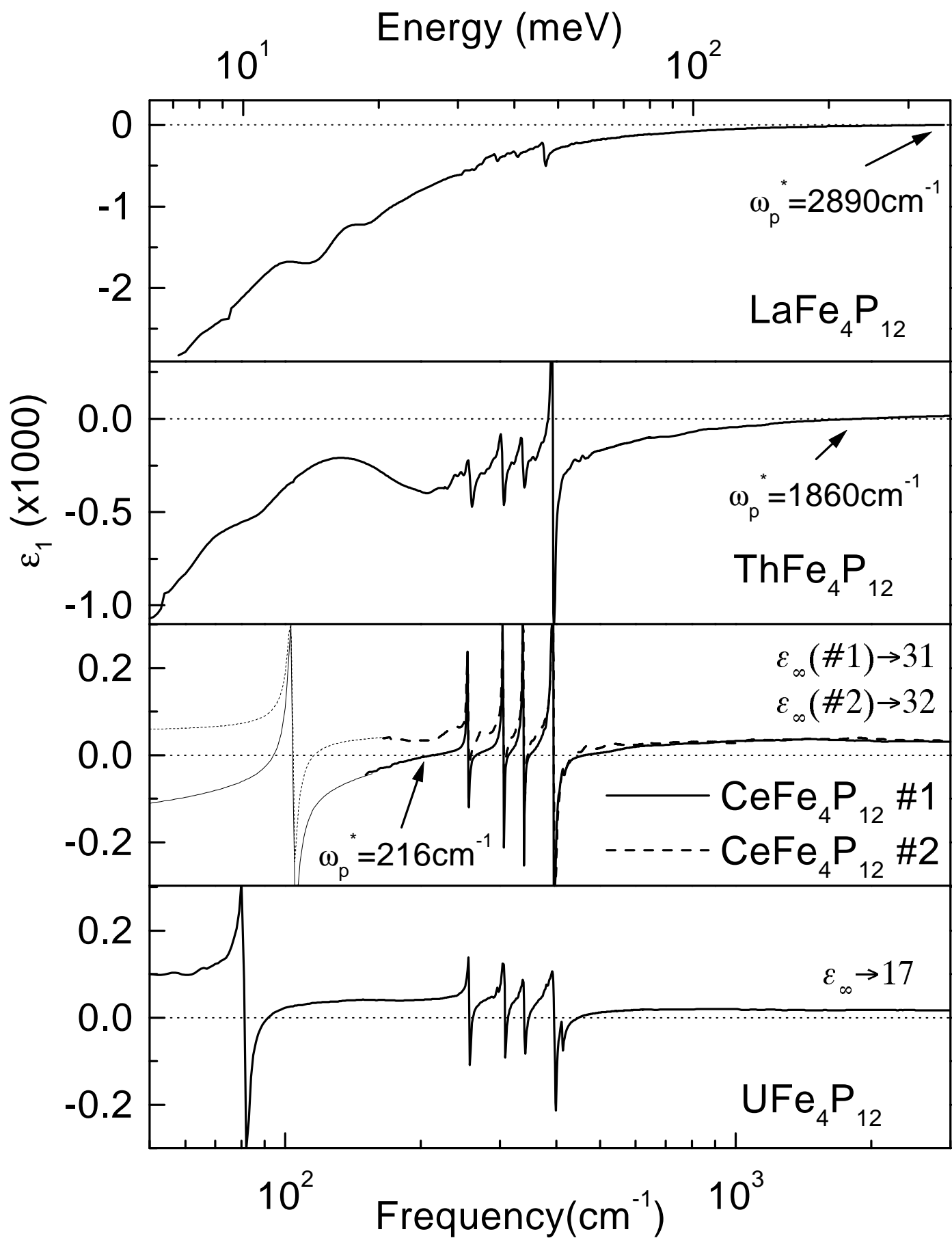


Figure 6

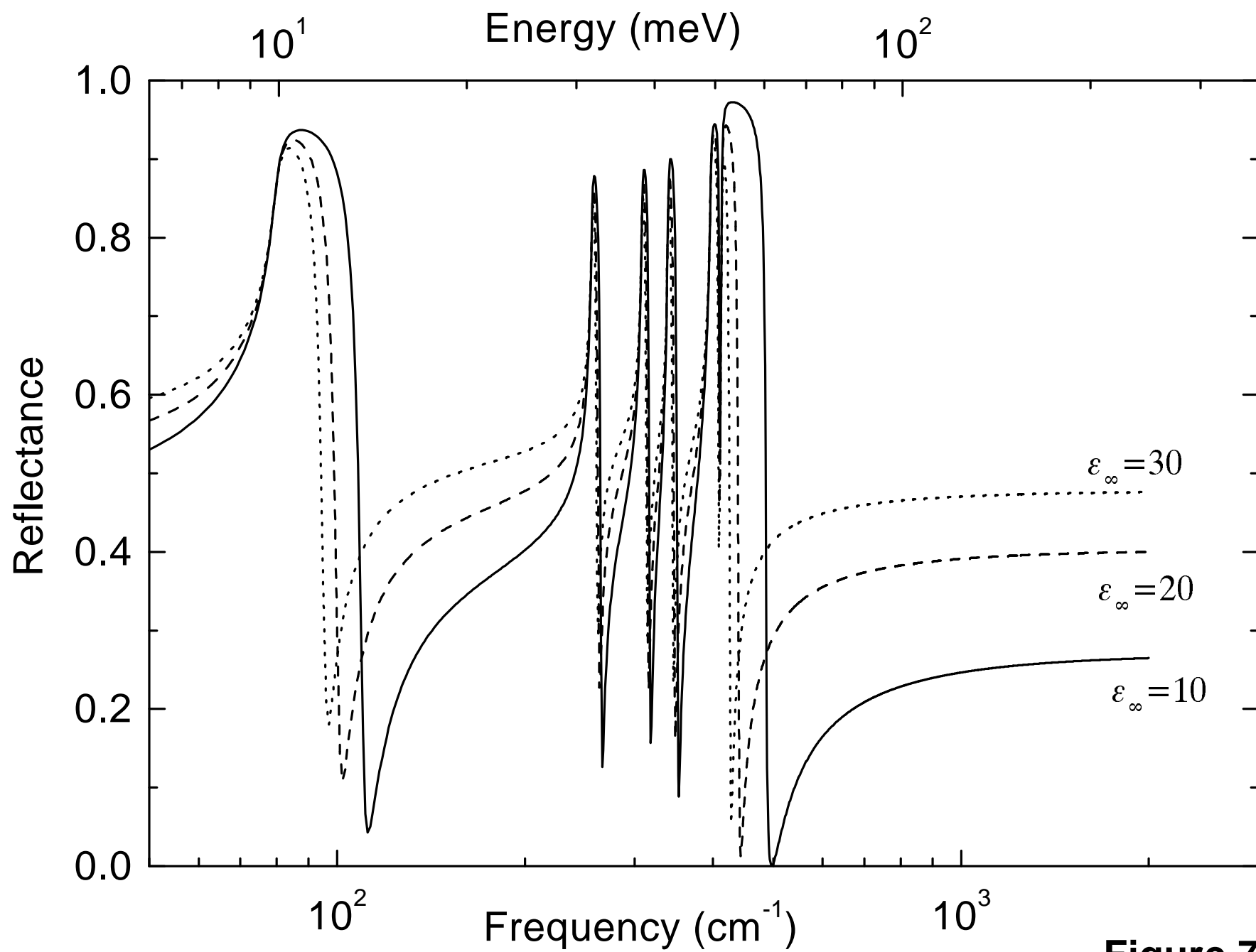


Figure 7